Study of the high-pressure helium phase diagram using molecular dynamics

2007 J. Phys.: Condens. Matter 19 016206

(http://iopscience.iop.org/0953-8984/19/1/016206)

INSTITUTE OF PHYSICS PUBLISHING JOURNAL OF PHYSICS: CONDENSED MATTER

J. Phys.: Condens. Matter **19** (2007) 016206 (9pp) doi:10.1088/0953-8984/19/1/016206

Study of the high-pressure helium phase diagram using molecular dynamics

L Koči[1], **R Ahuja**[1,2], **A B Belonoshko**[2,3] **and B Johansson**[1,2]

[1] Condensed Matter Theory Group, Department of Physics, Uppsala University, Box 530, S-751 21, Uppsala, Sweden
[2] Applied Materials Physics, Department of Materials Science and Engineering, The Royal Institute of Technology, S-100 44, Stockholm, Sweden
[3] Condensed Matter Theory, Alba Nova University Center, Physics Department, The Royal Institute of Technology, S-100 44 Stockholm, Sweden

Received 25 October 2006
Published 7 December 2006
Online at stacks.iop.org/JPhysCM/19/016206

Abstract

The rich occurrence of helium and hydrogen in space makes their properties highly interesting. By means of molecular dynamics (MD), we have examined two interatomic potentials for ^{4}He. Both potentials are demonstrated to reproduce high-pressure solid and liquid equation of state (EOS) data. The EOS, solid–solid transitions and melting at high pressures (P) were studied using a two-phase method. The Buckingham potential shows a good agreement with theoretical and experimental EOS, but does not reproduce experimental melting data. The Aziz potential shows a perfect match with theoretical melting data. We conclude that there is a stable body-centred-cubic (bcc) phase for ^{4}He at temperatures (T) above 340 K and pressures above 22 GPa for the Buckingham potential, whereas no bcc phase is found for the Aziz potential in the applied PT range.

1. Introduction

The properties of hydrogen and helium at high density are of great interest as these elements constitute 95% of the matter in the solar system [1]. Planets such as Jupiter and Saturn are believed to consist mainly of these two substances [2]. In order to build models for these planets, accurate equation of state data are required. For decades, the crystal structure, phase diagram and equation of state of helium have been investigated with experimental [3–5] and theoretical methods [6–8]. The diamond-anvil cell (DAC) measurements for the ^{4}He EOS shows a face-centred-cubic (fcc) to body-centred-cubic (bcc) phase transition prior to melting with a triple point (fcc–bcc–fluid) near $T = 300$ K and $P = 16$ GPa [5, 6]. This triple point was confirmed by Levesque *et al* [9]. The occurrence of a bcc phase could be explained by its higher entropy in comparison with the fcc phase, compensating the higher internal energy of the bcc structure [10]. Therefore, the Helmholtz free energy can be lower for the bcc phase.

However, the bcc phase was questioned by Loubeyre *et al* [11], who found the triple point to be fcc–hcp (hexagonal-close-packed)–fluid at about the same conditions. In this paper, we have used two interatomic potentials to perform molecular dynamics (MD) simulations for a wide range of temperatures and pressures to study phase transitions and melting points. The melting temperature T_m for a pressure P is defined by the condition where the Gibbs free energy of the solid and liquid are equal [12], i.e.

$$G_{\text{solid}}(P, T_m) = G_{\text{liquid}}(P, T_m). \tag{1}$$

This form is known as the *two-phase* method [13], reported to accurately determine the melting temperatures at a specific pressure [14]. We have also performed first-principles (*ab initio*) MD calculations based on density functional theory (DFT) in order to check the classical MD calculations based on empirical potentials. These techniques are described in the following section. Then, the results are presented, followed by a discussion and conclusions.

2. Methods

2.1. The models

First-principles (*ab initio*) methods are constantly developing [15–17], and benefit from the inclusion of electronic interaction, compared to classical methods. However, first-principles MD are computationally demanding, requiring long simulation times. Empirical potentials have functional forms which can be tuned to mimic to the maximum possible degree the energies and forces predicted by electronic structure techniques. By this semiempirical approach, the number of atoms included in the simulations can be significantly increased. However, as the parameters are tuned to experimental data, the method suffers if data are scarce. By fitting first-principles results to a classical model, one can combine the advantageous aspects of the first-principles as well as the semiempirical methods. Then, a classical MD simulation can be performed to operate on a big system. Several attempts have been made to test simple semiempirical pair potentials to match experimental He data [18, 19]. In this work, two interatomic potentials and parameter settings for ^{4}He were considered, namely the exponential-six (exp-6) potential from Ross and Young [1] and the Aziz [20] potential. The exp-6 potential is defined as

$$\Phi(r) = \epsilon \left\{ \frac{6}{\alpha - 6} \exp\left[\alpha\left(1 - \frac{r}{r_m}\right)\right] - \frac{\alpha}{\alpha - 6}\left(\frac{r_m}{r}\right)^6 \right\}, \tag{2}$$

where r is the interatomic distance and α, ϵ and r_m are adjustable parameters. The potential was for convenience converted to an equivalent Buckingham form,

$$V(r) = -\frac{A}{r^6} + B\mathrm{e}^{-Cr}, \tag{3}$$

with A, B and C as adjustable parameters. The parameters were fitted to equation of state data of high-pressure solid and liquid helium [2], using full-potential linear muffin-tin orbital electron band theory calculations. For the liquid, a variational hard-sphere perturbation theory was used to calculate the free energies, referring to the repulsive potential $\Phi_0(r) = \epsilon(\sigma/r)^{12}$. For the calculation of the solid free energies, quasi-harmonic lattice dynamics with anharmonic corrections were used. The model is expected to be valid at high pressures, but not for very low pressures, where quantum effects dominate the solid state properties. However, the melting curve of He at room temperature is only modestly influenced by quantum effects [9]. Furthermore, for rare gases, no electrons are available for bonding and atoms are attracted to each other through van der Waals forces. The parameters for the exp-6 potential together with the converted Buckingham parameters are presented in table 1.

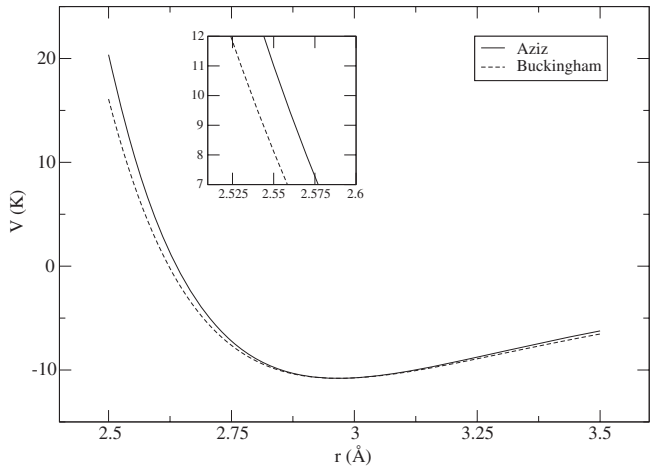

Figure 1. The Buckingham [1] and Aziz [20] potentials as a function of interatomic distance. Their discrepancy lies mainly in the part of small interatomic distances, where the stiffer Aziz potential has a higher repulsion than the softer Buckingham potential, shown in the inset.

Table 1. Exponential-6 potential parameters [2] and converted Buckingham potential parameters.

α	ϵ/k (K)	r_m (Å)	A	B	C
13.1	10.8	2.9673	113.09	37101	4.4148

Table 2. Aziz potential parameters [20].

A	α	C_6	C_8	C_{10}	D	ϵ/k (K)	r_m (Å)
$0.5449e^6$	13.353	1.373	0.425	0.178	1.241	10.8	2.9673

The Aziz potential is based on a combination of *ab initio* calculations of the self-consistent-field Hartree–Fock repulsion between closed shell systems, an empirical estimate of the correlation energy and semiempirically determined dispersion coefficients C_6, C_8 and C_{10}. It has the form

$$V^*(x) = Ae^{-\alpha x} - \left(\frac{C_6}{x^6} + \frac{C_8}{x^8} + \frac{C_{10}}{x^{10}}\right) F(x), \tag{4}$$

where

$$F(x) = \begin{cases} e^{(-\frac{D}{x}-1)^2} & \text{for } x < D \\ 1 & \text{for } x \geqslant D \end{cases}$$

and $x = r/r_m$. The parameters in equation (4) are presented in table 2. The discrepancy between the two interatomic potentials is shown in figure 1. The repulsive wall for interatomic distances smaller than r_m is stiffer for the Aziz potential in comparison to the Buckingham potential, clearly shown in the inset.

2.2. Technical details

The Moldy package [21] was used for the simulations, performed in the NPT ensemble (constant number of particles together with constant pressure and temperature). Periodic

boundary conditions were applied, meaning that if a particle leaves the simulation box, an identical particle enters on the other side. The simulation results with the chosen model of atomic interaction depend on several parameters such as the initial atomic configuration, the number of the time step n, the number of atoms N and the cutoff r_{cutoff}. By varying these parameters, we found that reliable results could be obtained with $n = 20\,000$ time steps, $N > 1500$ and $r_{\text{cutoff}} = 6$ Å. The cutoff roughly corresponds to the inclusion of the seventh-nearest neighbour. Furthermore, a strict cutoff was applied, meaning that all interactions between pairs of sites within the cutoff were included.

The density functional theory (DFT) calculations in this work were performed using the Vienna *ab initio* simulation package (VASP) [22, 23]. The generalized-gradient approximation (GGA) [24] was used as the exchange–correlation function.

3. Results

The radial distribution function $g_n(r)$ depends on temperature and density. Therefore, it serves as a helpful indicator of the phase assumed by the system in the MD calculations. In this work, the function was used to determine the different structures (bcc, fcc or liquid) as a function of temperature and pressure. The $g_n(r)$ function is defined in the following way: over an interval of n time steps of integration of the equations of motion, the mean volume V_n and the mean number of atoms N_n, at a distance between r and $r + \mathrm{d}r$ from an atom, are calculated. Then, $g_n(r)$ is given by

$$g_n(r) = \frac{N_n(r)V_n}{4\pi r^2\,\mathrm{d}r\,N}. \tag{5}$$

To visualize the bcc/fcc discrepancy by means of the $g_n(r)$, a perfect bcc lattice consisting of 1024 atoms was created by multiplying the bcc unit cell containing two atoms eight times ($2 \times 8 \times 8 \times 8$) in each of the three orthogonal directions. To resemble the density of the substance at the simulation conditions, the density was set to $\rho = 6.44$ Å^3/atom. One lattice was simulated with constant pressure and constant temperature (NPT) at 16 GPa and 200 K, whereas a second and a third identical lattice were simulated at higher temperatures of 300 and 425 K, respectively. The radial distribution function $g_n(r)$ was evaluated for the three simulations after 20 000 time steps and is shown in figure 2.

The number of neighbours for the first six shells are 12, 6, 24, 12, 24 and 8 for the fcc phase and 8, 6, 12, 24, 8 and 6 for the bcc phase. In figure 2, the arrows from below indicate the peak positions in a perfect bcc lattice, whereas the arrows from above indicate perfect fcc peaks. The first peak for the 200 K simulation is clearly higher and more narrow than that of the simulation performed at 300 K. The number of nearest neighbours in combination with the positions of the arrows indicate an fcc structure in the 200 K simulation and a bcc structure at 300 K. Furthermore, the $g_n(r)$ for the 300 K simulation shows a minimum at 4.6 Å, which can be related to few atoms in the fifth and sixth shells for the bcc phase. The fcc lattice has peaks at the third and fourth shells, manifesting in peaks for the 200 K simulation at 3.6 Å and 4.25 Å. A molten configuration is identified by a damped, oscillating behaviour of $g_n(r)$, clearly shown by the 425 K simulation (2).

To initiate the setup for the two-phase simulations, two perfect fcc lattices containing 864 atoms each were constructed, as the four-atom fcc unit cell was multiplied six times in the three orthogonal directions ($4 \times 6 \times 6 \times 6$). The lattice parameter $a = 3.03$ Å was chosen to represent the approximate lattice parameter at the pressure and temperature range ($P = 8$–40 GPa, $T = 100$–500 K) simulations. One of the lattices was simulated at $P = 17$ GPa and $T = 450$ K to transform into a molten configuration. The solid and molten structures were put together with

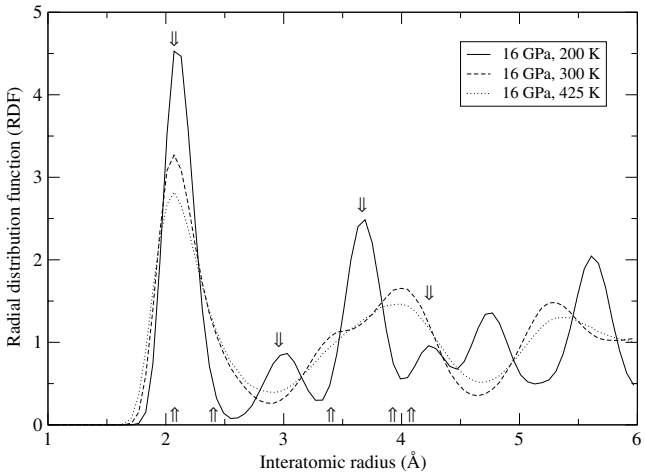

Figure 2. The radial distribution function for three NPT simulations with the Buckingham potential [1] at 16 GPa, 200 K; 16 GPa, 300 K and 16 GPa, 425 K. The arrows from below indicate the peak positions in a perfect bcc lattice, whereas the arrows from above indicate perfect fcc peaks. The correspondence between the arrows and the peaks from the simulations clearly separates the structures: the low-temperature simulation (200 K) results in an fcc configuration, whereas a higher temperature (300 K) implies a solid–solid phase transformation to the bcc structure before melting (425 K).

a small spacing in a simulation box, letting the lower part of the box be molten and the upper part be solid, as shown in figure 3. Starting from this configuration, the MD simulations result in a monophase. If the temperature is below T_{m}, the phase will crystalline whereas the phase will be liquid if the temperature is above T_{m}. By narrowing the interval, the melting temperature can be estimated at the specific pressure in the simulation. Belonoshko [13] explained the two-phase simulation method in detail, and its successful application for a number of systems has been reported [17, 25].

The equation of state (EOS) data shown in figure 4 show the pressure as a function of volume for the two-phase setup at 300 K with the Buckingham potential. There is a good match with the EOS results from Ross and Young [1], using the same potential. The discrepancy between Aziz and Buckingham results in the EOS is due to the stiffer Aziz potential.

The low-pressure behaviour of He is shown in figure 5. The Buckingham potential underestimates the volume at a given pressure and temperature with at most 5% compared to Young *et al* [2]. Comparing the Aziz and Buckingham melting curves with the data of Ross and Young [1], Loubeyre and Hansen [10] and Mao *et al* [26], the Aziz potential shows a better agreement to the referred data, shown in figure 6. At the same pressure, the Buckingham potential melts at a lower temperature than the Aziz potential due to its softer potential shape.

By means of NPT calculations for the two-phase system described for several pressures and temperatures, the melting and phase diagram with the Buckingham potential is shown in figure 7. To establish the configuration (crystal structure or liquid) from the simulation results, the $g_n(r)$ function was used as previously described. For low pressures, an increase in temperature implies a transition from the fcc crystal to a liquid structure. For higher pressures, the fcc phase transforms into the bcc structure before reaching the liquid phase at higher temperatures. Although starting from a setup with the fcc and liquid configurations, the bcc structure is more favourable than any of these at certain temperature and pressure conditions, implying that its Gibbs free energy is indeed lower. For the Aziz potential, no bcc phase is

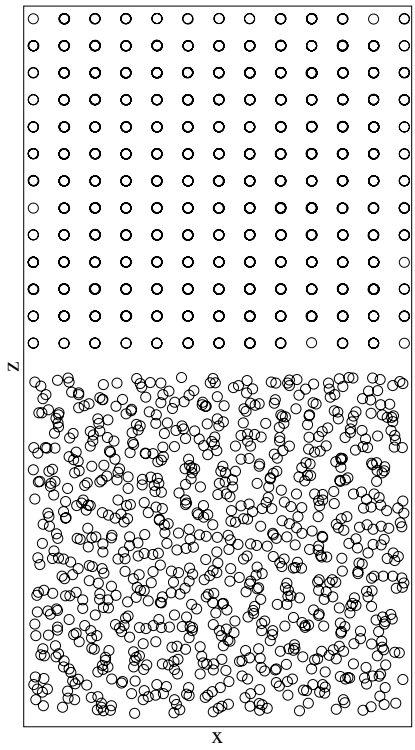

Figure 3. Two-phase setup where 864 atoms in an fcc structure are placed on top of 864 atoms in a molten structure (for enhanced readability, the figure has been plotted in two dimensions with the x and z axes). Starting from this configuration, the MD simulations result in a monophase. If $T < T_m$, the phase will be crystalline whereas the phase will be liquid if $T > T_m$. By narrowing the interval, the melting temperature can be estimated at the specific pressure in the simulation.

found for the pressure and temperature range shown in figure 7, nor for higher pressures and temperatures, following the melting curve up to 25 GPa.

4. Discussion

The Buckingham [1] and Aziz [20] models studied in this work are two-body models, in practice limited to rare gases. However, as the Buckingham potential parameters are developed from experimental data, many-body effects are incorporated implicitly in the model. The match with the *ab initio* data in figure 4 is almost perfect at higher pressures. At lower pressures, the *ab initio* calculations overestimate the pressure compared to the potential and experiments. This could be due to the limitation of DFT to accurately describe the van der Waals forces [27]. The omitting of three-body terms is discussed by Levesque *et al* [9], reporting the effects of the terms to be small for the rare gases in general, and for He in particular. The three-body forces are most likely to be very close in magnitude in a liquid and a solid. Therefore, the forces should not have a major impact on the equality of the Gibbs energies, determining the melting. The difference in the results of the two models originates from the stiffness of the Aziz potential shown in figure 1. This implies a lower compressibility (figure 4) and higher melting temperatures (figure 6). As Belonoshko [14] has reported the ability to accurately determine

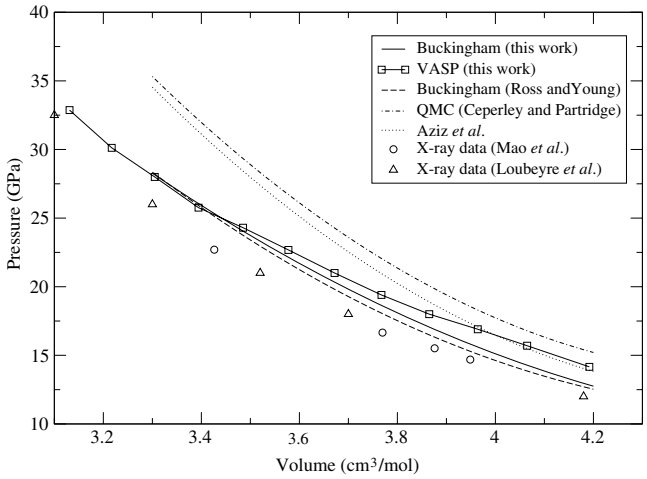

Figure 4. Pressure–volume equation of state for the Buckingham potential (this work) and the VASP calculations (this work). The experimental equation of state data at 300 K [11, 26] are shown as triangles and circles, respectively. The lines correspond to theoretical calculations, also from Mao *et al* [26] based on the pair potentials by Ross and Young [1], Ceperley and Partridge [8], and Aziz *et al* [20].

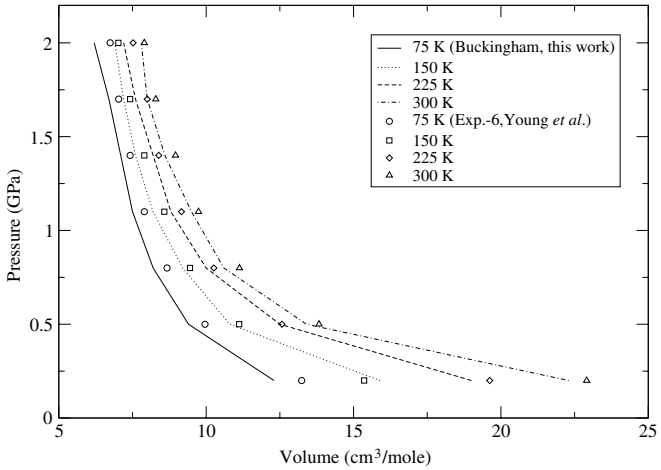

Figure 5. Pressure–volume equation of state for liquid He with the Buckingham potential [1] at 75, 150, 225, and 300 K. The symbols correspond to theoretical calculations with the exponential-6 potential [2], whereas the lines correspond to this work. The experimental data [3], serving as the reference for the Young *et al* parameter fitting, almost coincide with the exponential-6 data and are therefore omitted in the plot.

melting temperatures at specific pressures by the two-phase method, this study emphasizes that the Aziz model more correctly reproduces the melting curve compared to the Ross and Young model. The existence of an fcc–bcc transition in ^{4}He at the conditions studied is therefore not very likely, considering the results obtained with the Aziz potential. However, it is still possible that the Ross and Young model is doing better for solids, which could result in an fcc–bcc transition.

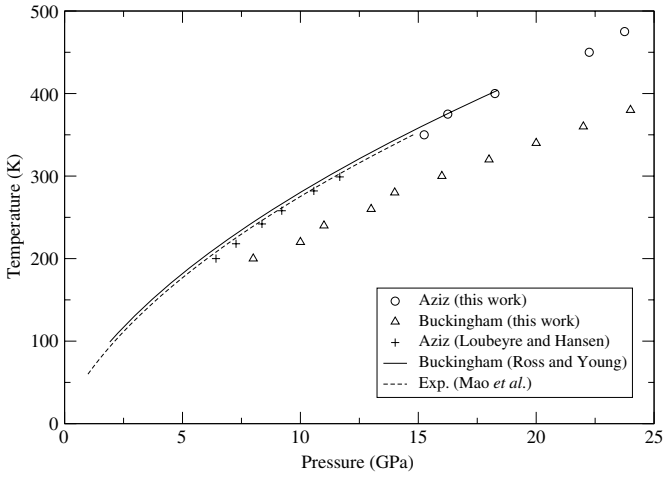

Figure 6. The two-phase melting with the Buckingham [1] and Aziz [20] potentials (this work), and the melting curves from Ross and Young [1], Loubeyre and Hansen [10] and Mao *et al* [26].

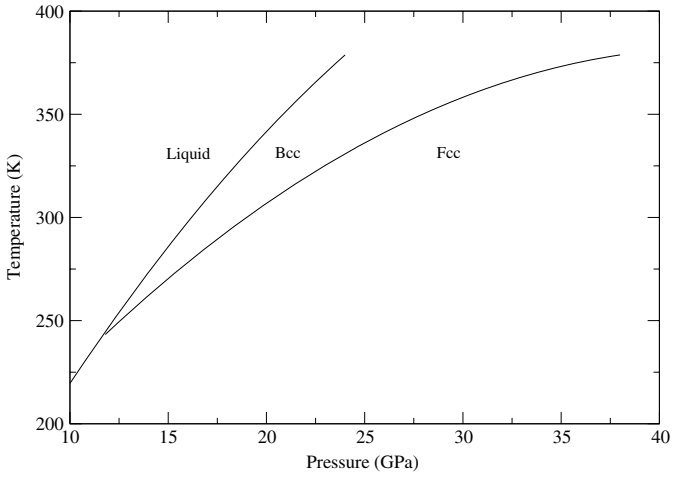

Figure 7. Phase boundaries as a result of two-phase simulations with the Buckingham potential [1]. In the initial configuration, 864 atoms in an fcc phase were placed on top of 864 atoms in a molten structure, as shown in figure 3. For lower pressures, the melting implies a transition from the fcc crystal to a liquid structure. For higher pressures, the fcc phase transforms into the bcc phase before reaching the liquid phase at higher temperatures. The bcc structure was sporadically observed at a pressure as low as 12 GPa. However, as the gap between the fcc structure and the liquid in the pressure and temperature range is small, the determination of the structure is difficult. By increasing the temperature and pressure, observations from 22 GPa and 340 K more consistently revealed the bcc phase.

5. Conclusions

We have compared the Buckingham potential [1] and the Aziz potential [20] for ^{4}He with MD simulations using a two-phase method. We have found that the Buckingham potential reproduces experimental and theoretical EOS data well. Furthermore, starting from the fcc and liquid two-phase configurations, there is a clear solid–solid transformation into the bcc

structure. Although the bcc structure is observed already at 12 GPa, the gap between the liquid and the fcc structure is small, making reliable structure determinations difficult. However, above 22 GPa and 340 K, the bcc structure was clearly observed. Due to the softness of the Buckingham potential compared to the Aziz potential, the melting occurs at lower temperatures compared to experiment. The Aziz potential overestimates the pressure at low densities from the EOS, but shows excellent agreement with theoretical melting data. Furthermore, the potential does not show a bcc structure between the fcc structure and the liquid configuration.

Acknowledgments

The authors are thankful to K Refson for the Moldy software package. This work was supported by the Swedish Research Council (VR).

References

[1] Ross M and Young D A 1986 *Phys. Lett.* A **118** 463
[2] Young D A, McMahan A K and Ross M 1981 *Phys. Rev.* B **24** 5119
[3] Mills R L, Liebenberg D H and Bronson J C 1980 *Phys. Rev.* B **21** 5137
[4] Franck J P and Daniels W B 1980 *Phys. Rev. Lett.* **44** 259
[5] Besson J M, LeToullec R, Loubeyre P, Pinceaux J P and Hansen J P 1984 *High Pressure in Science and Technology* vol 2, ed C Homan, R K MacCrone and E Whalley (Amsterdam: North-Holland)
[6] Loubeyre P, Besson J M, Pinceaux J P and Hansen J P 1982 *Phys. Rev. Lett.* **49** 1172
[7] Chang S Y and Boninsegni M 2001 *J. Chem. Phys.* **115** 2629
[8] Ceperley D M and Partridge H 1986 *J. Chem. Phys.* **84** 820
[9] Levesque D, Weis J-J and Klein M L 1983 *Phys. Rev. Lett.* **51** 670
[10] Loubeyre P and Hansen J P 1985 *Phys. Rev.* B **31** 634
[11] Loubeyre P, LeToullec R, Pinceaux J P, Mao H K, Hu J and Hemley R J 1993 *Phys. Rev. Lett.* **71** 2272
[12] Alfè D, Vočadlo L, Price G D and Gillan M J 2004 *J. Phys.: Condens. Matter* **16** 973
[13] Belonoshko A B 1994 *Geochim. Cosmochim. Acta* **58** 4039
[14] Belonoshko A B 2002 *J. Chem. Phys.* **117** 7233
[15] Stixrude L, Cohen R E and Singh D J 1994 *Phys. Rev.* B **50** 6442
[16] Söderlind P, Moriarty J A and Wills J M 1996 *Phys. Rev.* B **53** 14 063
[17] Belonoshko A B, Ahuja R and Johansson B 2000 *Phys. Rev. Lett.* **84** 3638
[18] Pollock E L, Bruce T A, Chester G V and Krumhansl J A 1972 *Phys. Rev.* B **5** 4180
[19] Etters R D, Raich J C and Cochran C 1972 *J. Low Temp. Phys.* **9** 53
[20] Aziz R A, Nain V P S, Carley J C, Taylor W L and McConville G T 1979 *J. Chem. Phys.* **70** 4330
[21] Refson K 2003 *Moldy User's Manual*
[22] Kresse G and Hafner J 1993 *Phys. Rev.* B **47** 558
[23] Kresse G and Furthmueller J 1996 *Phys. Rev.* B **54** 11169
[24] Perdew J P, Burke K and Ernzerhof M 1996 *Phys. Rev. Lett.* **77** 3865
[25] Belonoshko A B, Ahuja R, Eriksson O and Johansson B 2000 *Phys. Rev.* B **61** 3838
[26] Mao H K, Hemley R J, Wu Y, Jephcoat A P, Finger L W, Zha C S and Bassett W A 1998 *Phys. Rev. Lett.* **60** 2649
[27] Rovira C 2005 *Methods Mol. Biol.* **305** 517